Elements of the quantitative rescattering theory

IOP Publishing Journal of Physics B: Atomic, Molecular and Optical Physics
J. Phys. B: At. Mol. Opt. Phys. **51** (2018) 104001 (15pp) https://doi.org/10.1088/1361-6455/aabaa2

Elements of the quantitative rescattering theory

C D Lin[1], Anh-Thu Le[1], Cheng Jin[2] and Hui Wei[1]

[1] Department of Physics, Cardwell Hall, Kansas State University, Manhattan, KS 66506, United States of America
[2] Department of Applied Physics, Nanjing University of Science and Technology, Nanjing, Jiangsu 210094, People's Republic of China

E-mail: cdlin@phys.ksu.edu

Received 22 January 2018, revised 14 February 2018
Accepted for publication 29 March 2018
Published 25 April 2018

Abstract

In this contribution to celebrate '25 years of recollision physics', we reflect on how the quantitative rescattering (QRS) theory was developed during the 2007–9 period. A short summary on how QRS was applied to different rescattering phenomena, including the probing of target structure or the characterization of the driving laser pulse is then given. The success of the QRS theory was built upon the recollision model proposed 25 years ago.

Keywords: strong field physics, recollision physics, quantitative rescattering theory, high-energy above-threshold ionization, high-order harmonic generation

(Some figures may appear in colour only in the online journal)

1. Introduction

In this special issue of '25 years of recollision physics', the authors would like to reflect on the circuitous tour that lead us to the quantitative rescattering (QRS) theory in 2009 when the acronym was coined [1, 2]. Of course, by 2009, rescattering theory has been in existence for more than fifteen years. In particular, in its simplest form, the three-step model—ionization, propagation and recollision, is the 'standard model' of any talks on strong field rescattering physics, in no difference from the introduction of three generations of quarks and leptons in any high-energy physics seminars. The concept of the three-step model, first appeared in the early work of of Kuchiev in 1987 [3], became generally received in the strong field community after 1993 following the seminal papers of Krause *et al* [4] and Corkum [5]. The theoretical foundation of rescattering was significantly further advanced following the semiclassical treatment of Lewenstein *et al* [6] in 1994, where the rescattering model was 'extracted' from an approximate solution of the time-dependent Schrödinger equation (TDSE). This important paper demonstrated the connection between the classical three-step model and the quantum theory of the strong field approximation (SFA), from the early work of Keldysh [7], Faisal [8] and Reiss [9]. In the ensuing years, the rescattering model was widely used to 'interpret' strong field experiments or numerical results obtained from solving the TDSE, such as the approximate cutoff energies in high-order harmonics or in high-energy photoelectrons, but it does not offer a means to make quantitative predictions. Thus the recollision theory was incomplete.

We entered the strong field physics late, around 2002. By then most experiments on atomic targets are already quite well understood, or at least they can be calculated by solving the TDSE using a single active electron model (SAE). At the time, ionization from a diatomic molecule was taken as the interference of the ionization amplitudes from the two atomic centers [10]. This approach has some success, but tearing a molecule into its atomistic components is not desirable. By considering the well-established description that an electron in a molecule is represented by a molecular orbital, in collaboration with Xiao-Min Tong and Zengxiu Zhao, our first paper in strong field physics was to extend the ADK theory of Ammosov *et al* [11] for strong field ionization of atoms to molecules. Since molecular orbitals are directional, the resulting MO-ADK theory [12] provides a simple method to calculate the dependence of tunneling ionization rate on the alignment angle of a molecule with respect to the polarization axis of the laser field.

The MO-ADK theory demonstrates that alignment-dependent ionization rates of molecules are proportional to the electron density distribution of the highest occupied

molecular orbital (HOMO) from which the electron was removed. It turns out that measuring the alignment-dependent ionization rate of a molecule is not trivial because a laser can also align a molecule before ionization. The effect of the latter is mitigated by using a very short laser pulse as shown in the pioneering work of Alnaser *et al* [13].

This initial exercise leads us to recognize the need to bring in theoretical tools developed in atomic and molecular physics into strong field physics, in particular, for molecules, to take advantage of the various quantum chemistry codes such as Gaussian and GAMESS to obtain HOMO wavefunctions in order to extract the structure parameters in the MO-ADK theory. Subsequently, in 2005, Zhou *et al* [14, 15] extended the high-harmonic generation theory of Lewenstein *et al* [6] for atoms to molecular targets. Such a simple theory was used to interpret the alignment-dependent HHG data for N_2 molecules from Itatani *et al* [16] and later for O_2 and CO_2 from Sakai *et al* (2005) [17, 18]. In the meanwhile, standard tools in conventional atomic and molecular physics laboratories like COLTRIMS and VMI for measuring the energy and momentum distributions of electrons and ions were quickly becoming familiar components in most ultrafast laboratories. Thus, in the first decade of the 21st century, we witnessed not only the 'discovery' of attosecond pulses [19, 20], but also the renaissance of strong field physics which was to evolve into a powerful method for probing atoms and molecules with temporal resolution of tens of femtoseconds. For the latter to become practical, however, the theory has to be able to provide means to extract target structure information from the strong field experiments.

2. Basic theoretical tools in strong field physics

Since the early days, one of the main quantum mechanical frameworks for studying strong field physics is the strong field perturbation expansion method. The first-order term of the expansion has been called the SFA. It will be called SFA1 in this article to distinguish it from the next order, which is to be called the SFA2. The SFA1, which is closely related to the KFR theory, describes direct ionized electrons that emerge with energy up to $2U_p$, where U_p is the ponderomotive (or quiver) energy of a free electron over one optical laser cycle. The SFA2 is responsible for the rescattered electrons, in particular, for electrons with kinetic energy beyond about $4U_p$ to about $10U_p$. These high-energy above-threshold-ionization (HATI) electrons are from laser-driven returning electrons that have been rescattered by the parent ion into the backward direction. The SFA2 term is also responsible for high-order harmonic generation (HHG) where the returning electrons recombine with the ion with the excess energy emitted as high-energy photons. Another rescattering phenomenon is the nonsequential double ionization (NSDI) where the returning electron knocks out another electron from the ion at recollision to result in doubly charged ions with the release of two free electrons.

In all three rescattering phenomena, the returning electrons come from the initial ionization of a neutral atom or molecule. These electrons are then driven by the oscillating laser field and may return as an electron wave packet to recollide with the parent ion. This sequence constitutes the first and second steps of the three-step model. In the third step, depending on the nature of electron–ion collisions, it leads to HATI, HHG, or NSDI phenomena. Even though electron–ion collisions are rarely studied experimentally in the laboratory, collisions between electrons with neutral atoms or molecules have been extensively studied experimentally and theoretically in the past six decades. Electron collisions are powerful tools for probing the structure of single atoms or molecules. Thus one would expect that HATI, HHG, and NSDI spectra contain structure information of the target atom or molecule. On the other hand, it is crucial to point out one important distinction: HATI, HHG, and NSDI are electron–ion collisions occurring in the presence of the laser field. In the three-step model, it does not address how the presence of the laser field would modify the conventional field-free electron–ion collisions. It is often generally expected that laser field would modify field-free electron–ion collisions but the question left unanswered for more than a decade.

To compare a strong field ionization theory directly with experiment is difficult since the laser parameters in a focused laser beam are generally not precisely determined. However, for a one-electron atom or a many-electron atom modeled in the SAE model, accurate solution of the TDSE is possible. Such TDSE results can be used as 'experimental data' to calibrate simple models such as the rescattering model. Once the time-dependent wavefunction is available, the HATI and HHG spectra can be easily calculated. In fact, such a TDSE solver was already available by early 1990s. Clearly NSDI cannot be calculated within the SAE model. For the time being, we will not consider NSDI.

Since the three-step model has been identified as the main mechanism of the rescattering phenomena and its main features can be calculated from the SFA2 theory (or the Lewenstein model), it is tempting to build an improved theoretical model that can 'repair' the inherent errors within the SFA2. This was the route that we took to develop the QRS theory.

To simplify the discussion below, we first write down the well-known equation for SFA1 for describing the emission of direct electrons by the intense laser, and SFA2 for the mission for HATI electrons. The SFA2 can also be written down for the HHG processes if the recollision is replaced by recombination.

The probability amplitude for obtaining photoelectron with final momentum $\mathbf{k}$ within the SFA1 is

$$A_1(\mathbf{k}) = -\mathrm{i}\int_{-\infty}^{\infty} \mathrm{d}t \,\langle \chi_{\mathbf{k}}(t)|H_{\mathrm{i}}(t)|\ \Psi_0(t)\rangle \tag{1}$$

and for SFA2 is

$$A_2(\mathbf{k}) = -\int_{-\infty}^{\infty} \mathrm{d}t \int_{t}^{\infty} \mathrm{d}t' \int \mathrm{d}\mathbf{p} \langle \chi_{\mathbf{k}}(t')|V|\ \chi_{\mathbf{p}}(t')\rangle \times \langle \chi_{\mathbf{p}}(t)|H_i(t)|\ \Psi_0(t)\rangle. \tag{2}$$

In the above, Ψ_0 and $\chi_{\mathbf{k}}$ are the ground state and Volkov state wavefunction, respectively. $H_i = \mathbf{r}\cdot\mathbf{E}(t)$ is the laser's

interaction with an atom or molecule in the length gauge, with **E** being the laser's electric field. V is the 'effective' electron-parent ion potential.

For HHG, the time-dependent laser-induced dipole in the SFA2 model is written as

$$\mathbf{D}(t) = -\mathrm{i}\int_{-\infty}^{t} \mathrm{d}t' \int \mathrm{d}\mathbf{p}\, \mathbf{d}^*(\mathbf{p} + \mathbf{A}(t))\mathbf{E}(t') \cdot \mathbf{d}(\mathbf{p} + \mathbf{A}(t'))\mathrm{e}^{-\mathrm{i}S(\mathbf{p},t,t')} + \text{c.c.} \quad (3)$$

Here $\mathbf{d}(\mathbf{p}) = \langle \mathbf{p}|\mathbf{r}|\Psi_0\rangle$ is the dipole transition matrix element between the bound state and a continuum state, and S is the action. We note that the induced dipole in the frequency domain would have an additional integration over the 'recombination' time t. This would bring the final equation for HHG in close resemblance to equation (2) for HATI.

3. The QRS model

3.1. The pre-QRS period

Before 2008 there have already been quite a number of experimental and theoretical papers on HATI and HHG spectra. For example, in 1993 Yang *et al* [21] studied the angular distributions of high-energy photoelectrons on Xe and Kr atoms using 50 ps, 1.05 μm lasers. It was observed that strong peaks appeared at large angles near 45° off the polarization axis in Xe, but not in Kr. These strong peaks were interpreted as due to large-angle back-rescattering of the returning electrons by the ionic core. In 2004, Spanner *et al* [22] theoretically addressed 'Reading diffraction images in strong field ionization of diatomic molecules'. Using photo-electron angular distributions calculated from solving the TDSE for H_2^+ molecular ions, they analyzed the procedures that would allow them to recover the undistorted diffraction image from the laser generated electron spectra. The method was too complicated and it was not put in actual application to experimental data.

On the HHG front, harmonic spectra generated from aligned N_2 molecules were reported in Itatani *et al* in 2004 in Nature [16] under the title 'Tomographic imaging of molecular orbitals'. In the experiment, N_2 molecules are partially aligned and HHG spectra are measured as a function of the alignment angle of the molecules with respect to the laser polarization direction. The authors assumed that the harmonic spectra polarized along the x-direction can be expressed as

$$S(\omega, \theta) = N(\theta)^2\omega^4\, |a[k(\omega)]\mathbf{d}(\omega, \theta)|^2. \quad (4)$$

Here $N(\theta)$ is the ionization amplitude, $a[k(\omega)]$ is the returning electron wave packet, $\mathbf{d}(\omega, \theta)$ is the dipole transition amplitude between the HOMO and the continuum state, ω is the energy of the emitted photon, and θ is the angle between the laser polarization and the molecular axis.

Under the assumption that the returning electron wave packet is not sensitive to the target, the wave packet can be factored out when the molecular harmonic spectra are compared to the harmonic spectra of a reference atom. Thus the magnitude of the transition dipole of a molecule can be expressed as

$$|\mathbf{d}(k, \theta)| = N(\theta)^{-1}|\mathbf{d}_{\text{ref}}(k)|\, \sqrt{S(\omega, \theta)/S_{\text{ref}}(\omega)}. \quad (5)$$

In the experiment, the reference atom is Ar, which has nearly the same binding energy as N_2. The expression (4) was an ansatz based on the three-step model. In Itatani *et al* [16] the photo-recombination transition dipole (PRTD) moment in the length gauge is written as

$$\mathbf{d}(\omega, \theta) = (2\pi)^{-3/2}\int \mathrm{d}\mathbf{r}\Psi_0(\mathbf{r}; \theta)\mathbf{r}\exp[\mathrm{i}k(\omega)x]. \quad (6)$$

In equation (6), Ψ_0 is the ground state wavefunction and $\exp[\mathrm{i}k(\omega)x]$ is a plane wave representing the wavefunction of the continuum electron. To get better results, the kinetic energy of the electron was taken as $k^2/2 = \hbar\omega$ in Itatani *et al*. This last expression clearly violates Einstein's relation for photoelectric effect: $k^2/2 = \hbar\omega - I_p$, with I_p being the ionization energy of the ground state orbital. In equation (6) the continuum electron is represented by a plane wave. Based on equation (6) and a similar expression for polarization along the y-direction, a two-dimensional Fourier transform was then used to extract the ground state wavefunction $\Psi_0(x, y)$.

The tomographic imaging method of extracting the ground state molecular orbital by Itatani *et al* [16] has created a great deal of excitement in the strong field community, but it also has drawn a lot of skepticism from the atomic and molecular physics community. The wavefunction of a molecular orbital is a mathematical construct in quantum mechanics and in principle is not measurable. Besides, the ground state alone does not give information about the spectroscopy nor the interatomic separation of the molecule. In Le *et al* [23], the limitations of the tomographic imaging method were discussed. It is clear that the use of equations (5) and (6) is equivalent to the calculation of HHG spectra using the SFA2 (Lewenstein) model. Such a simple model is known to be unable to describe the HHG spectra of atoms already.

3.2. Extracting returning electron wave packet from SFA2 and from TDSE for HATI electrons

In conventional atomic and molecular physics, photoelectron angular distributions are often measured for the study of the structure of atoms and molecules. For multiphoton ionization of atoms by linearly polarized lasers, the ATI electrons are strongly peaked along the polarization axis with the increase of the number of photons absorbed. For rare gas atoms, results from TDSE calculations have shown that at low energies the momentum distributions exhibit fan-like structure [24] and a semi-empirical scaling law for the number of nodes in the angular distributions has been identified [25]. The existence of scaling means that there is little target structure information contained in the low-energy electron spectra. This is in strong contrast to one-photon ionization where photoelectron angular distributions are very different for different targets.

In 2007, we began to study two-dimensional high-energy ATI photoelectron momentum distributions using the SFA2

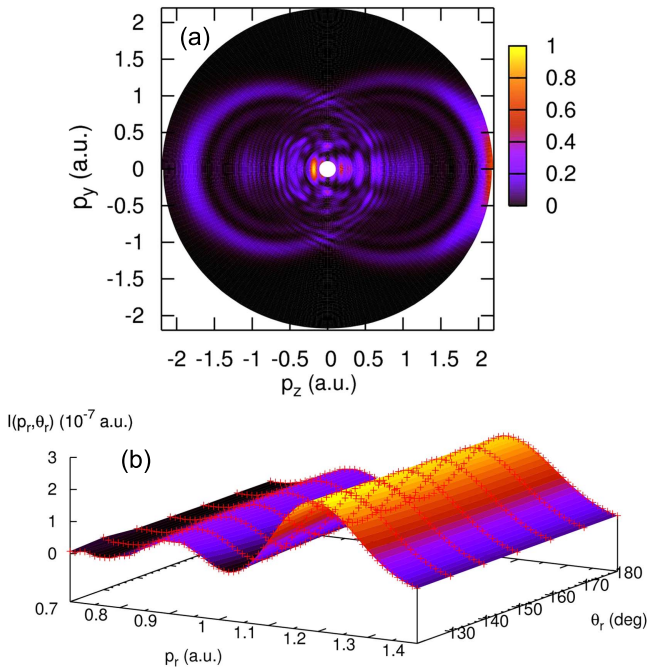

Figure 1. (a) Two-dimensional photoelectron momentum distributions parallel (denoted as p_z) and perpendicular (p_y) to the laser polarization axis for atomic hydrogen ionized by a few-cycle, 800 nm laser pulse obtained using SFA2 theory. (b) The wave packets of the returning electrons are shown to be independent of the direction of the photoelectrons, i.e., the scattering angles. This condition has to be satisfied if the recollision model is correct. Reprinted figure with permission from [26]. Copyright (2007) by the American Physical Society.

model and solving the TDSE [26]. Since the yields of HATI electrons are very small compared to direct electrons at lower energies, we first investigated the normalized momentum spectra, i.e., the total integrated angular distributions at each photoelectron energy is renormalized to one. A typical result of this representation from SFA2 is shown in figure 1(a). At large momenta, a semi-circle on each side along the laser polarization axis is clearly visible. The center of the semi-circle is shifted from the origin of the momentum spectra along the polarization axis. The electrons along each semi-circle are readily understood as resulting from the elastic scattering of an electron by the ion core and the shift of the center is due to the additional momentum gained by the electron as it emerges from the laser field. The momentum gain is given by the vector potential of the laser field at the time of recollision, i.e.,

$$\mathbf{p} = -\mathbf{A}_r + \mathbf{p}_r. \tag{7}$$

This transformation is similar to a two-body collision seen in the laboratory frame versus in the center-of-mass frame, with $-\mathbf{A}_r$ being the 'velocity' of the center of mass with respect to the laboratory frame. To describe a two-body collision, the scattering is better formulated in the center-of-mass frame even though the measurement is performed in the laboratory frame. Thus to understand recollision dynamics in a strong laser field, the electron momentum to consider is $\mathbf{p}_r$. It is related to the momentum of the photoelectron in the laboratory frame by equation (7).

To support that photoelectrons along each ring satisfying equation (7) can indeed be interpreted as due to elastic collision of the returning electron with a momentum $\mathbf{p}_r$, it is imperative to demonstrate that the photoelectron distributions along the semi-circle can be expressed as

$$I(p, \theta) = W(p_r)\sigma(p_r, \theta_r), \tag{8}$$

where the momentum and angle in the two frames are related by equation (7). Note that the right-hand side of equation (8) is the standard expression for defining the differential cross sections (DCS) for the collision of an electron with an atomic ion without the presence of the laser. This is a very strong statement of the third step of the three-step model: the DCS in equation (8) is the field-free DCS. Both $W(p_r)$ and $\sigma(p_r, \theta_r)$ can only be extracted from equation (8) in the region of $\{p, \theta\}$ where equation (8) holds.

Mathematically it is always possible to define

$$I(p, \theta) = W(p_r, \theta_r)\sigma(p_r, \theta_r). \tag{9}$$

To establish that equation (8) is not limited to SFA2, we need to verify that it also holds for solutions obtained from the TDSE. For this purpose, we obtain $I(p, \theta)$ from solving the TDSE equation. To obtain $\sigma(p_r, \theta_r)$, we solve the standard (laser-free) time-independent Schrödinger equation for electron–parent ion scattering. Within the SAE picture, the same model potential is used in both TDSE and scattering calculations. From these calculations, the ratio $W(p_r, \theta_r) = I(p, \theta)/\sigma(p_r, \theta_r)$ is obtained. If the resulting $W(p_r, \theta_r)$ is independent of θ_r, then we can write $W(p_r, \theta_r) = W(p_r)$ such that $W(p_r)$ behaves like a beam of incident electrons with momentum p_r. For convenience, $W(p_r)$ is called the returning electron wave packet. Note that there are different concepts of electron wave packet used in the literature which might bear no resemblance to the concept of the wave packet used in the QRS model. Within the QRS, the returning electron wave packet is defined as if it is prepared at the asymptotic distance from the target.

To get $\mathbf{A}_r$ in equation (7), classical equation of motion of a free electron in an oscillatory laser field is solved to find the returning electron with momentum $\mathbf{p}_r$ at the time t_r when it reaches the ion core. Here $\mathbf{A}_r$ in equation (7) is the vector potential at the time of recollision. Even though in general there are two return times for the electron to return with the same p_r, it is safe to just use the return time for the long-trajectory electrons. These are electrons born at the time when the electric field is large and thus have much higher ionization probability. In addition, for HATI electrons, p_r is large where the vector potential for the long and short trajectory electrons differ only slightly. The wave packet $W(p_r)$ obtained this way is called $W_{\mathrm{tdse}}(p_r)$. If $I(p, \theta)$ is calculated from the SFA2, then $\sigma(p_r, \theta_r)$ is the DCS calculated in the Born approximation. The wave packet obtained from the similar ratio will be called $W_{\mathrm{sfa}}(p_r)$.

Figure 1(b) shows the typical $W(p_r, \theta_r)$ calculated from the SFA2. Indeed it exhibits no dependence on θ_r, thus the validity of equation (8) is established for the SFA2 theory, indirectly verifying the validity of the three-step model. However, equation (8) should also be checked against real

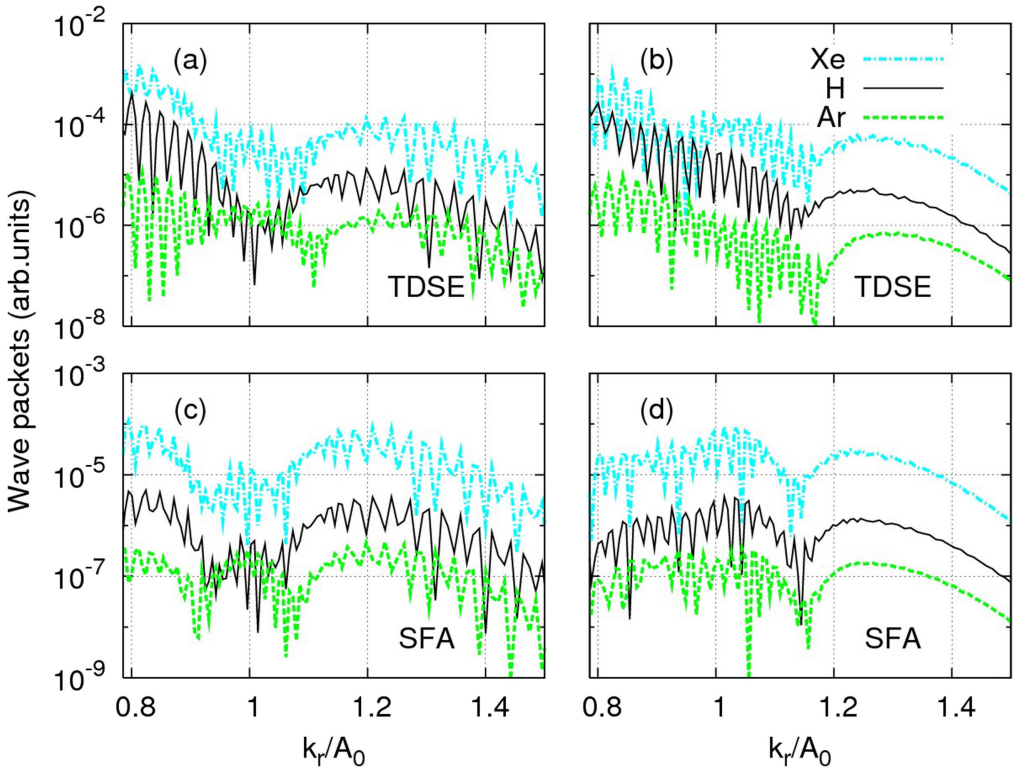

Figure 2. Electron wave packets extracted from TDSE (upper frames) and from SFA2 (lower frames) for single ionization of H, Ar, and Xe in an eight-cycle pulse at peak intensity of 1.0×10^{14} W cm^{-2}. Left panels (right panels) show the left-side (right-side) wave packet with photoelectron momentum $k_z < 0$ ($k_z < 0$), respectively. These figures show that the wave packets are relatively independent of the targets but strongly dependent of the lasers. The slight shifts of the wave packets among the targets in the TDSE results illustrate the shift of the electron momentum distributions due to the residual electron–ion interaction. Such small shifts are ignored in the QRS theory. Reprinted figure with permission from [1]. Copyright (2009) by the American Physical Society.

$I(p, \theta)$ obtained from TDSE against real field-free DCS $\sigma(p_r, \theta_r)$ for each strong laser field. For atoms under the SAE model both calculations can be readily accurately calculated. Following the same procedure, the $W_{\rm tdse}(p_r)$ can also be shown to be independent of θ_r. Moreover, it has the same p_r dependence as the one extracted from the SFA2, except for a small shift along the p_r axis. Figure 2 compares the $W(p_r)$ extracted from TDSE and from SFA2 for three targets, H, Ar and Xe, under the same laser pulse. Except for an overall normalization due to the incorrect ionization rate of the SFA theory, the wave packets from SFA2 and from TDSE for each target look very similar. There is a very small overall shift in the momentum distribution. Such a shift is due to the electron–ion core potential in the TDSE calculation that is neglected in the SFA2 model. Within TDSE, the extracted wave packets for the different targets also differ somewhat since the core potentials are different. The differences in the SFA2 may be attributed to the different ionization potential. For practical purpose, such small shift is not significant compared to other uncertainty in the experiment and is neglected in the simple QRS theory.

It is prudent to emphasize once again that the wave packets $W(p_r)$ and field-free DCS $\sigma(p_r, \theta_r)$ are extracted quantities in reference to the laser frame. In particular, $W(p_r)$ is not a wave packet that can be directly measured experimentally. For each p_r, $W(p_r)$ is the weight of the scattering wave (sw) which has an asymptotic momentum p_r in the direction of the returning electron, since $\sigma(p_r, \theta_r)$ is defined with respect to the same sw. This clarification is essential in order to identify $\sigma(p_r, \theta_r)$ as the field-free DCS. Note that the $W(p_r)$ is given in the momentum space. To know the wave packet in the coordinate space, the phase of the returning electron wave packet has to be determined. Such information is not available in the photoelectron spectra. Experiments claiming the measurement of the returning electron wave packets are inconsistent with the QRS model.

3.3. Retrieving laser-free DCS from two-dimensional HATI electron momentum spectra

Returning to equation (8) again, it says that for a fixed p_r, one can extract the DCS, $\sigma(p_r, \theta_r)$, from the photoelectron momentum spectra for a range of θ_r. Since equation (8) is consistent with the recollision model, one would not use small θ_r angles where the 2D momentum spectra are contaminated by direct electrons. Without knowing $W(p_r)$ for a given p_r, one can extract the relative angular dependence, i.e., the DCS, for field-free electron–ion collision directly. The extracted DCS should be identical to the DCS for field-free electron–ion collisions, which can be measured in the laboratory, or from solving the time-independent Schrödinger equation. Indeed equation (8) is an extremely strong statement on the validity of the recollision model. It also states that the extracted DCS is independent of the lasers.

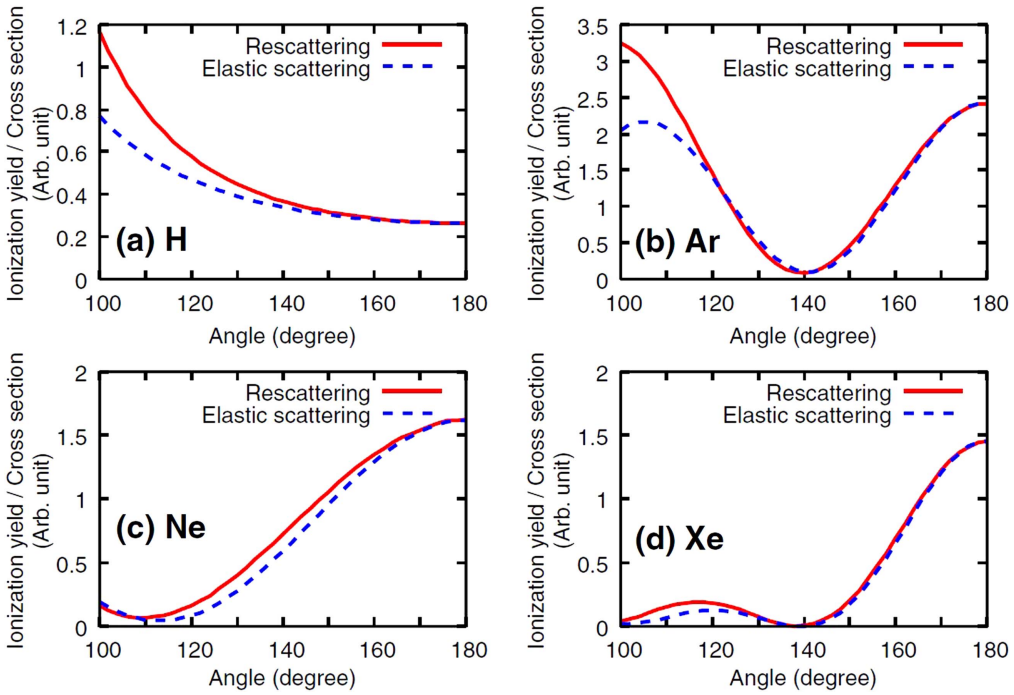

Figure 3. Angular distributions of photoelectrons for returning electrons that has the maximal kinetic energy of $3.2U_p$ for H, Ar, Ne, and Xe. Shown are the electron–ion elastic scattering DCS extracted from the HATI momentum spectra (red lines) as compared to DCS obtained from electron–ion collisions at the same kinetic energy. The good agreement demonstrates that equation (8) can be used to extract field-free elastic electron–ion collision DCS from the HATI momentum spectra. Reprinted figure with permission from [27]. Copyright (2008) by the American Physical Society.

In figure 3 we compare the DCSs of H, and of Ne, Ar, and Xe atoms under the SAE model. They are extracted from the HATI momentum spectra calculated by solving the TDSE of these atoms in a 5 fs, 800 nm laser pulse at an intensity of 1.0×10^{14} W cm^{-2}. The θ_r range where the two DCSs are in good agreement extends from about 120°–180°, confirming that equation (8) is valid for backscattered angles. The angular range can be extended to smaller angles if longer wavelength lasers are used. These results established that structure information of the target under laser-free conditions can be retrieved from laser generated two-dimensional high-energy ATI electron momentum spectra. We checked this as a general statement and many additional tests have been made on TDSE results. As a side remark, in our initial test, we found discrepancy in Ne. We were confident enough to attribute that the discrepancy comes from the lack of convergence in the TDSE calculation instead of the failure of equation (8). Once more accurate TDSE calculations were carried out, equation (8) is confirmed for Ne as well.

Equation (8) shows that the normalized retrieved field-free DCS depends only on the value of p_r, and not on the details of the laser pulses used, including laser's intensity, wavelength, pulse duration and carrier-envelope phase (CEP), so long that p_r is within the rescattering region and below the cutoff energy. This has been tested on many simulations for atoms. Such independence is important if the DCS extracted indeed is to be independent of the applied lasers. Thus in equation (8), the wave packet $W(p_r)$ contains all the information about the lasers. The target dependence enters only in the total electron flux through the initial ionization rate. In other words, the shape of $W(p_r)$ is largely independent of the target.

The separability of equation (8) states that the 2D momentum distributions of HATI electrons can be written as a product of two terms, one term is mostly (except normalization factor) determined by the laser, and the other depends entirely on the target (except the p_r should be such that its kinetic energy is below $3.2U_p$). Another salient feature of equation (8) is that the shape of $W(p_r)$ obtained from TDSE and from SFA2 differs mostly only in the overall normalization. Thus in the QRS model the HATI momentum spectra in the rescattering region can be rewritten as

$$I_{\rm qrs}(p,\,\theta) \sim W_{\rm sfa}(p_r,\,\theta_r)\sigma_{\rm sw}(p_r,\,\theta_r), \tag{10}$$

where the normalization factor can be fixed by multiplying the ratio of the ionization probability obtained from ADK or from the PPT theory [28] with respect to the one calculated from the SFA1. Equation (10) has the form of the three-step model where $W_{\rm sfa}(p_r)$ includes the first and second steps of ionization and propagation, and the third step is the elastic scattering DCS $\sigma_{\rm sw}(p_r,\,\theta_r)$ between electron and the ion calculated using accurate sw. Equation (10) is based on the rescattering model. It is in a form that can be used to calculate HATI momentum spectra. Since $I(p,\,\theta)$ thus calculated is at a level close to the TDSE solutions, we called equation (10) the QRS theory in Chen *et al* [1], to emphasize its distinction from the conventional three-step model, or the rescattering model, that does not offer quantitative predictions. In QRS, the DCS is to be calculated using the correct continuum sw. Such DCS calculations have been carried out in conventional

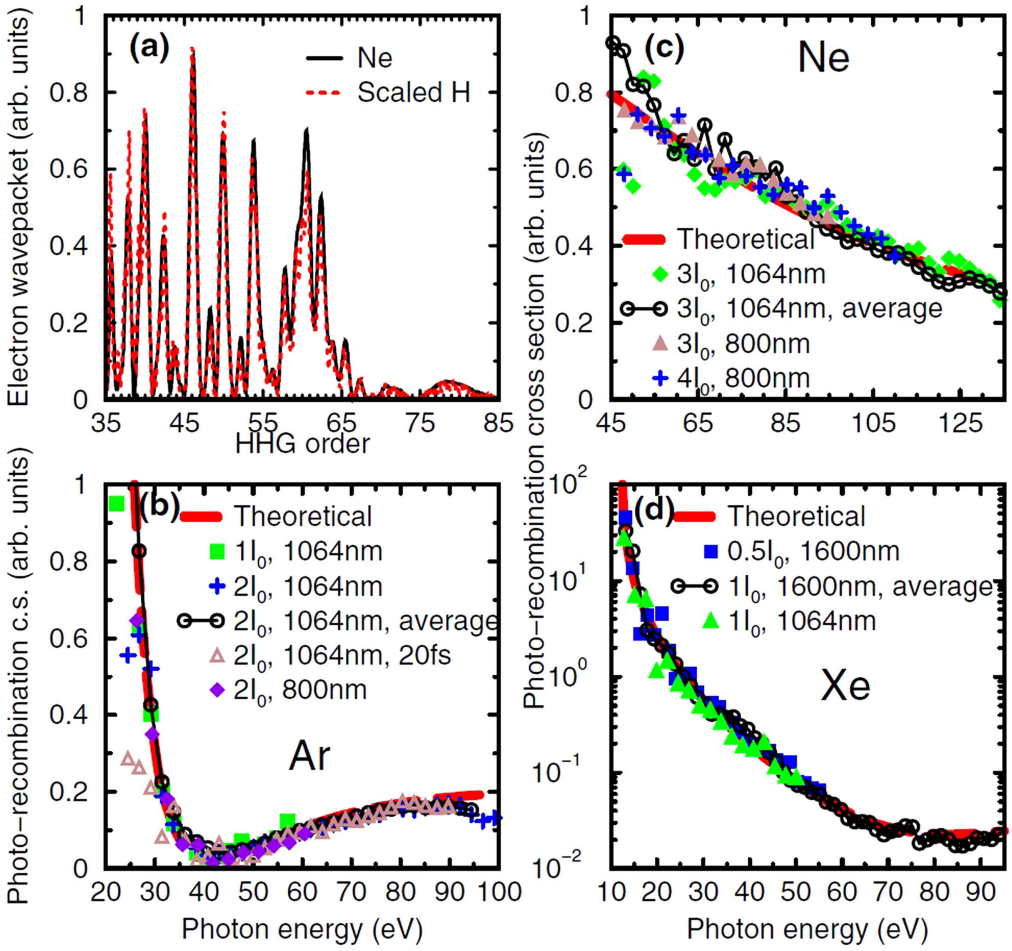

Figure 4. (a) Comparison of electron wave packet extracted from the HHG spectra of Ne and scaled H generated by a 5 fs laser pulse. (b)–(d) Extracted photo-recombination cross sections from the HHG of Ne, Ar and Xe using different laser pulses. These results demonstrate that the wave packets do not depend significantly on the target, and that photo-recombination cross sections of the target are independent of the lasers used. These results demonstrate that field-free photoionization cross sections can be extracted from HHG spectra of each atom. Reprinted figure with permission from [27]. Copyright (2008) by the American Physical Society.

atomic and molecular physics. In more advanced theories, many-electron correlation effects are often included in such DCS calculations. Within the QRS model, many-electron correlation effect can be directly included by using the DCS obtained from such many-body theories.

The separable form of equation (10) makes the QRS model a powerful tool for calculating the elementary 2D momentum spectra of HATI electrons. Since the DCS is independent of laser, it only has to be calculated once for a range of the returning electron energies below the maximal $3.2U_p$ cutoff. Since the SFA2 calculations and the DCS in the Born approximation can all be calculated in a few seconds only, equation (10) can be performed over hundreds of laser intensities easily with small increment of intensity in each step, thus making it rather simple to account for volume integration in QRS-based calculations.

3.4. QRS theory for HHG

Once the QRS model is established for HATI electrons, it is straightforward to follow the same procedure to generalize it to the HHG process. Since high-order harmonics generated by a focused laser beam from each atom are added up coherently in the gas medium, equation (8) is generalized to the complex transition amplitudes

$$D(\omega) = a(\omega)d(\omega), \tag{11}$$

where $D(\omega)$ is the complex dipole moment of the laser-induced harmonic, $a(\omega)$ is the complex wave packet of the returning electron with kinetic energy $k^2/2 = \omega - I_p$ where I_p is the ionization energy, and $d(\omega)$ is the one-photon transition dipole matrix element under the field-free condition from the ground state to the continuum state. Since the cutoff energy of the harmonics is given by $3.2U_p + I_p$, we check the validity of the HHG spectra of two model atoms, one is a Ne atom under the SAE model and another is a scaled hydrogenic atom with an effective charge chosen such that the two targets have identical I_p. For simplicity, we just show the magnitude (modulus square of each quantity) of the electron wave packet and the PRTD that can be extracted from the harmonic spectra obtained by solving the TDSE equation.

Figure 4(a) [27] shows that the normalized electron wave packets obtained from the two targets under the same laser pulses are in good agreement, confirming that the electron

wave packets are the properties of the laser. In this example, the electron was ionized from the 1s orbital in the scaled hydrogen atom while for the model neon, it is ionized from the 2p orbital. Thus it demonstrates that the returning electron wave packet in the QRS model does not depend on the orbital symmetry of the ground state wavefunction. In figures 4(b)–(d), the photo-recombination cross sections for Ne, Ar, and Xe extracted from the HHG spectra are shown to be independent of the wavelength and intensity of the lasers used and they agree with the field-free photo-recombination cross sections. In fact, the phase of the atomic transition dipole $d(\omega)$ has also been extracted and shown in [29]. These calculations essentially established the correctness of equation (11) for atomic targets.

The validity of equation (11) for HHG extracted from TDSE and from the SFA2 allows one to calculate HHG spectral amplitudes of atoms within the SAE model from

$$D_{\rm QRS}(\omega) = a_{\rm SFA}(\omega) d(\omega). \tag{12}$$

Here $a_{\rm SFA}(\omega)$ can be obtained from solving the SFA2 for HHG (the Lewenstein model), or by solving TDSE for another companion atom, say the scaled hydrogen atom. Since the electron wave packet is made of single ionization from a many-electron atom, the many-electron effect is expected to be small. On the other hand, many-electron effects, such as intershell coupling, existence of resonances, are known to become important in some spectral region for some atoms. Such effects can be directly incorporated by using the PRTD $d(\omega)$ calculated from many-electron photoionization theory. For example, HHG from Xe atoms generated by 1825 nm lasers [30] have been obtained using transition dipole moment calculated from random phase approximation. Theoretically, many-body single-photon ionization theory is much simpler than the direct solution of the many-electron TDSE equations. In this respect, the HHG spectra can be used as a method of obtaining the broadband photoionization cross sections for probing the structure of the target. Conventional photoionization experiments are normally carried out with nearly monochromatic lights from synchrotron facilities. Such measurements provide high resolution spectra but only over a narrow energy regime.

3.5. Analytical derivation of the separability of harmonic emission using quantum orbits theory

The separability in equations (8) and (11) was postulated based on the rescattering model and then calibrated based on numerical results from solving the TDSE for HATI electrons and for HHG spectra for SAE model atom. Around 2008 such TDSE calculations were already quite common and highly accurate for atoms. Looking back, the modulus square of equation (11), in the form of equation (4), has already been used by Itatani *et al* [16]. After Morishita *et al* [27], there are other publications [31–34], which derived similar separable approximations like equations (8) and (11), for one-electron model atom where the electron sees a short-range potential, as for the case of a negative ion. While the details are different, all of such models are somewhat equivalent to the SFA2 theory where plane waves can be used to describe a continuum electron from a target with short-range potential. In fact, QRS was employed to calculate strong field photodetachment of negative ions in Zhou *et al* [35]. We note a quite recent work [36], in which the inclusion of the Coulomb tail was discussed.

Within the QRS approach, the separable approximation can be readily derived from the quantum orbits theory. The derivation below was first reported in [37]. We summarize it here as it would also give reader a glimpse of the semiclassical formulation of the classical three-step model for rescattering.

Starting with the standard Lewenstein (SFA2) model, the x-component of the induced dipole for harmonic generation by a linearly polarized laser can be expressed as

$$D_x(t) = -\mathrm{i}\int_{-\infty}^{t} \mathrm{d}t' \left(\frac{-2\pi\mathrm{i}}{t-t'-\mathrm{i}\epsilon}\right)^{3/2} d_x^*(p_s + A(t)) \times d_x(p_s + A(t'))E(t')\mathrm{e}^{-\mathrm{i}S(p_s,t,t')} + \mathrm{c.c.}, \tag{13}$$

where $d_x(p) = \langle p\mathbf{e}_x|x|g\rangle$ is the transition dipole moment, E is the electric field of the laser, S is the action, and the momentum p_s within the saddle point approximation is given by

$$\mathbf{p}_s = -\frac{1}{t-t'}\int_{t'}^{t} \mathbf{A}(t'')\mathrm{d}t''. \tag{14}$$

Equation (13) can be obtained from equation (3) after integrating over the intermediate continuum states using the saddle point approximation. The Fourier transform of $D_x(t)$ can be written as

$$D_x(\omega) = \int_{-\infty}^{\infty} D_x(t)\mathrm{e}^{\mathrm{i}\omega t}\mathrm{d}t, \tag{15}$$

where

$$D_x(\omega) = -\mathrm{i}\int_{-\infty}^{\infty}\mathrm{d}t\int_{-\infty}^{t}\mathrm{d}t'\left(\frac{-2\pi\mathrm{i}}{t-t'-\mathrm{i}\epsilon}\right)^{3/2} \times d_x^*(p_s + A(t))d_x(p_s + A(t'))E(t')\mathrm{e}^{-\mathrm{i}\Theta(p_s,t,t')}. \tag{16}$$

In the above equation,

$$\Theta(p_s, t, t') = S(p_s, t, t') - \omega t, \tag{17}$$

$$S(p_s, t, t') = \int_{t'}^{t}\mathrm{d}t''\left(\frac{1}{2}[p_s + A(t'')]^2 + I_p\right). \tag{18}$$

In the so-called quantum orbits theory, one applies the saddle point approximation to the two integrals over time. Assuming relative smoothness of the transition dipole as compared to the fast variation of the phase Θ, the saddle points satisfy $\partial\Theta/\partial t' = 0$ and $\partial\Theta/\partial t = 0$, which lead to

$$\frac{1}{2}[p_s + A(t')]^2 = -I_p \tag{19}$$

and

$$\frac{1}{2}[p_s + A(t)]^2 = \omega - I_p, \tag{20}$$

respectively. The saddle points t_s and t_s' are referred to as the recombination and ionization times, respectively. The saddle point approximation to equation (16) is then written as

$$D_x(\omega) = -\mathrm{i}\sum_s \sqrt{\frac{(2\pi\mathrm{i})^2}{\det(\Theta'')}}\left(\frac{-2\pi\mathrm{i}}{t_s - t_s'}\right)^{3/2} \times d_x^*(p_s + A(t_s))d_x(p_s + A(t_s'))E(t_s')\mathrm{e}^{-\mathrm{i}\Theta(p_s,t_s,t_s')}. \quad (21)$$

This equation expresses that the induced dipole is the sum of transitions due to separate individual trajectories (labeled by s). Taking into account the explicit forms of equations (19) and (20), the above equation can be further simplified to

$$D_x(\omega) = d_x^*(\sqrt{2(\omega - I_p)})d_x(\mathrm{i}\sqrt{2I_p}) \times \sum_s \frac{2\pi\varepsilon_s'\varepsilon_s}{\sqrt{\det(S'')}}\left(\frac{-2\pi\mathrm{i}}{t_s - t_s'}\right)^{3/2} E(t_s')\mathrm{e}^{-\mathrm{i}\Theta(p_s,t_s,t_s')} \equiv d_x^*(\sqrt{2(\omega - I_p)})w(\omega). \quad (22)$$

The final expression is now given as a product form. The photo-recombination dipole matrix d_x^* is to be evaluated at the kinetic energy of electrons at $k^2/2 = \omega - I_p$. The wave packet $w(\omega)$ is then given by the rest of the expression. It contains the initial ionization amplitude and summation of terms from each trajectory s in the electron wave packet. It can also be seen that the wave packet $w(\omega)$ contains parameters involving the laser only. The only 'structure' dependence occurs in the dipole moment $d_x(\mathrm{i}\sqrt{2I_p})$ that is related to the ionization amplitude.

The result from this 'derivation' confirms that the transition dipole $d_x^*(\sqrt{2(\omega - I_p)})$ indeed is not modified by the driving laser. It is easier to think that the recombination occurs in the laser frame where the transition dipole occurs under field-free condition, as in the conventional photo-recombination in the laboratory frame. In addition, it also confirms that the correct relation between k and ω is given by the Einstein equation $k^2/2 = \omega - I_p$, in contrast to $k^2/2 = \omega$ given in Itatani *et al* [16].

3.6. Generalization of the QRS to multi-color laser fields

The QRS model derived in the previous subsections for a single-color, linearly polarized pulse can be easily generalized to other laser fields in the spirit of the three-step model. This is expected since in the 'derivation' based on the quantum orbits theory, the only general assumption used was the slow change of the transition dipoles as compared to the fast variation of the action. For example, one can extend it to HATI spectra from two-color laser fields. The applications, according to the QRS, can only modify the wave packets but not the transition dipole or the scattering amplitude. The vector potentials at the return times can be calculated from the simple classical equation of motion of the electron in 1D. Most of the applications so far include long wavelength lasers up to a few microns, two-color fields with various combinations of intensities and their relative phase, or few-cycle pulses with varying CEP. In all of these cases, the electron is emitted and returns along the laser polarization axis.

In the case of elliptically polarized pulses as well as two-color orthogonally polarized pulses, it was also found that factorization in the spirit of the QRS is approximately valid

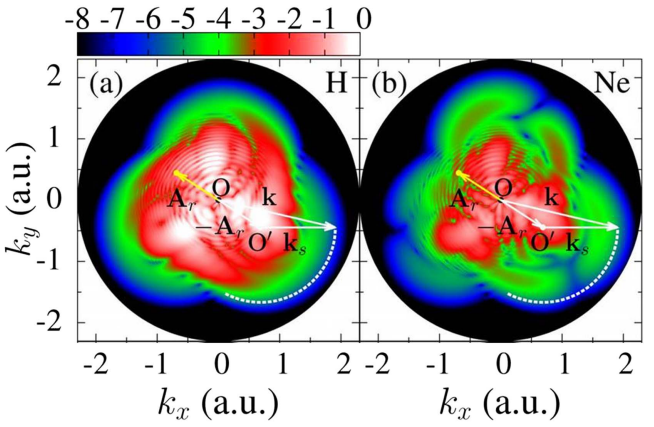

Figure 5. (a) and (b) 2D momentum spectra in xy plane from H and Ne($2p_-$), respectively. The dashed white circular arcs denote the region where electron yields are extracted in figure 6, for $k_s = 1.22$ a.u. Note that the color is in logarithmic scale. Reprinted figure with permission from [50]. Copyright (2017) by the American Physical Society.

[38–40]. Interested readers are referred to those works. Below we address a special case of two-color pulses which has attracted a great deal of interest quite recently. Namely, the case of two-color (ω-2ω) counter-rotating circularly polarized pulses (to be called bicircular pulses in the following). The interests were caused by the rich physics observed in experiments in both electron and HHG spectra [41–45]. In particular, with bicircular pulses, high-order harmonics has also been efficiently generated [41, 42], to provide a new table-top source of circularly polarized coherent light, ranging from extreme ultraviolet to soft x-ray up to 160 eV [43]. Quite recently, these harmonics have been demonstrated to be very sensitive to the electronic structure [46–48], thus providing a new technique in HHG spectroscopy. In essence, the technique relies on the factorization of HHG dipole. A detailed analysis of the validity of the QRS factorization for bicircular lasers is reported in [49].

In the following we analyze the validity of the QRS for electron spectra with bicircular pulses [50]. The analysis is based on the exact numerical solution of the TDSE. We choose the laser polarization to lie on the x–y plane. Clearly, once the electron is 'born' into the continuum, it will be driven by the laser field predominantly on the 2D plane instead of in the 1D direction as in the case of linearly polarized lasers. By using the classical equation of motion, one can calculate the trajectories of the electron in the continuum and find the returning direction of the electron. Upon recollision, the electron scatters in all directions. A cut on the x–y momentum plane is shown in figures 5(a) and (b) for H(1s) and Ne($2p_-$), respectively. In both targets we see a three-lobe structure instead of a 'two-lobe' structure as for the linearly polarized case. We remarks that the 2D momentum spectrum from Ne($2p_+$) looks quite similar to that of Ne($2p_-$). Also, due to our choice of the quantization axis along the z axis, the contribution from Ne($2p_0$) is negligible. Clearly, different targets have different imprints on the details of the lobes. Once the direction of the returning electron is found by classical or quantum orbits calculations, one can follow the

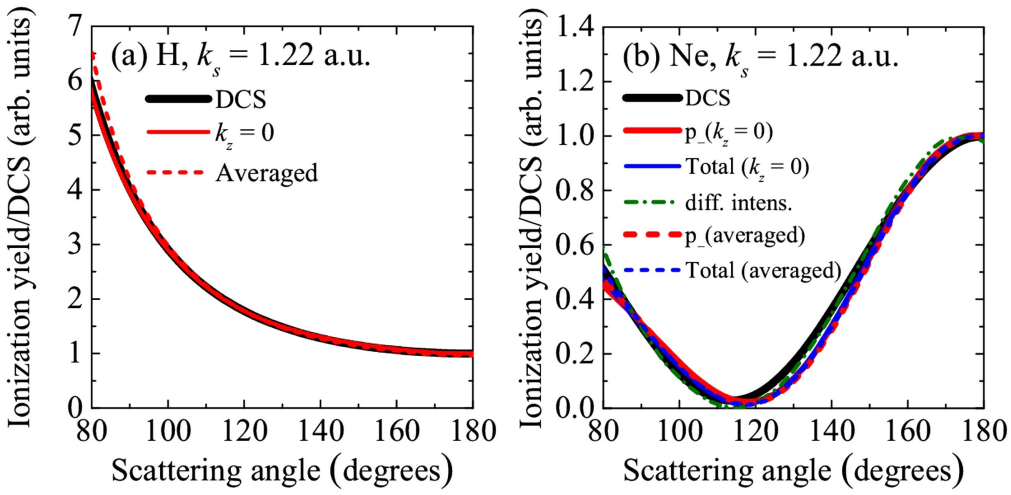

Figure 6. (a) and (b) Extracted yields along the white arcs shown in figure 5 with a scattering momentum $k_s = 1.22$ a.u., for H and Ne, respectively. Different extraction procedures were used (see the labels). The sum of yields from p_- and p_+ is labeled as 'total'. The averaged results from 3D momentum spectra are labeled as 'Total (averaged)'. The theoretical laser-free DCS is shown as a thick solid black line. The photoelectron yields have been normalized to that of the DCS near 180°. Reprinted figure with permission from [50]. Copyright (2017) by the American Physical Society.

QRS recipe to extract the electron signals at different angles for a fixed return energy. The results are shown in figures 6(a) and (b), for H(1s) and Ne($2p_-$), respectively. The signals agree very well with the DCS for each target. By changing laser parameters such as intensities and wavelengths, the momentum image is changed, but the shape of the extracted 'DCS' versus scattering angle at a fixed energy is unchanged. This clearly demonstrates the validity of the QRS.

The above analysis can be extended to the full 3D momentum image. In fact, it was found that once the return electron direction is known, the extracted DCS is independent of the scattering angle ϕ, as expected. As shown in figure 6 the averaged results from the 3D data are indeed nearly identical to the one extracted from the 2D data. More explicit evidences can be found in [50]. This result can be utilized to experimentally determine the electron return angle, if the laser parameters are not known accurately.

These newer results demonstrate that the QRS description is valid for a wide range of laser parameters, extending it to including lasers that are not linearly polarized. The only common requirement is that the relevant process, either HHG or HATI, is in the tunneling regime.

4. Remarks on further applications and limitations of the QRS theory

The QRS theory has been widely used for applications in strong field rescattering physics since 2008, in particular, to molecular systems for which most of the experiments have been carried out. More extensive discussions on the applications of the QRS theory can be found in authors' forthcoming book [51]. Here we only give a short summary without showing the results.

Based on equations (11) and (8), the essential ingredients for applying the QRS theory are the PRTD moment for the HHG process and the elastic electron–ion collision DCS for the HATI spectra. Both of them are familiar quantities widely studied in the past six decades in atomic and molecular physics and sophisticated computer codes, including treatment of many-electron correlation, have been developed. According to the QRS, the only nonlinear quantity is in the returning electron wave packet, in particular, the ionization step. The latter can be calculated using the SFA1 model and then use the ADK (or MO-ADK), or the PPT (or MO-PPT) theory to renormalize it to get accurate (absolute) wave packets if needed. Note that the QRS model is based on treating a 'rescattering event', i.e., the ionization, propagation, and recollision steps of a SAE, which was initially in a specific molecular orbital. In reality, the SAE model is an approximation; this assumption may become inadequate, especially for large complex molecules where many occupied molecular orbitals have nearly the same binding energies. Accurate calculations of PRTD and DCS are already quite complicated in such cases. On the other hand, QRS may still be carried out within the SFA2 model for 'qualitative diagnosis' in certain cases. For example, in dynamic systems such as in an isomerization process, when the interatomic distances are changed significantly, difference in the PRTD and DCS are likely reflected in the HATI and HHG spectra. For example, the alignment dependence of HHG signals are very different between acetylene and vinylidene in the SFA2 model, see Le *et al* [23]. By monitoring the HHG spectra in an isomerization process, it may provide a good estimate of the time it takes the system to complete an isomerization process.

We also note that the QRS theory is formulated in the energy domain, thus its predicted results are used to compare directly with experimental measurements. Unlike the classical three-step model, it does not offer 'experimental' time information. On the other hand, classical ionization and return times are used to relate the momentum of the electron in the laser

frame and in the laboratory frame, thus a qualitative statement about the 'time' is implied. Such a 'time' is not measured, thus assigning a precise 'time' in the recollision event, especially on attoseconds scale may be a bit too far-fetched. The subtlety of the wave packet $W(p_r)$ should also not to be ignored. It is given in the energy domain, which gives the amplitude of the wave packet when the electron momentum is p_r in the laser frame. The separable approximation in equation (8) or (11) cannot be viewed in the laboratory frame. In other words, to extract structure or laser information directly in the laboratory frame would be very complicated, if not impossible.

In the next four subsections, we give a few examples of the application of the QRS model.

4.1. Applications to HATI electron spectra and laser-induced electron diffraction (LIED)

There are very few quantum chemistry codes that can calculate accurate DCS for electron–ion collisions with molecules fixed in space, particularly for low-energy electrons below 50 eV or so where many-electron correlation effect in general is important. Since free molecules cannot be fixed in space, the measured HATI spectra are always averaged over the angular distribution. The same average has to be performed on theoretical HATI spectra as well. Up to now, most of the experimental HATI spectra from simple molecules like O_2, N_2, CO_2, and some hydrocarbon molecules are limited to isotropically distributed ones and only rarely have the results been compared to accurate calculations within the QRS scheme [52].

The DCS is generally easy to calculate for high-energy electrons, say, up to tens to hundreds keVs. For laser generated rescattering, however, the electron kinetic energy in the laser frame is limited to about $3.2U_p$, where U_p is proportional to the square of the wavelength of the driving laser. Thus, in principle, one can use long wavelength lasers to generate higher energy electrons. However, the yield of the returning electrons is unfavorably scaled like λ^{-5} [37, 53–56], thus at present it is not realistic to generate enough keV rescattering electrons for recollision events. On the other hand, in Xu *et al* [57], it was theoretically shown that HATI electrons generated by mid-infrared lasers can be used for electron diffraction to determine the bond length of molecules. Since HATI electrons are from backscattered elastic collision events by the returning electrons, the momentum transfer of a 100 eV electron would amount to the same momentum transfer as keV electrons that are forwardly scattered. In both cases the electron undergoes large momentum transfer, implying that they are deflected from a distance close to the nucleus of each atom in the molecule. At such short distances, the incident electron experiences the strong force from the nuclear charge and scattering by outer-shell electrons plays little role. Thus the scattering theory becomes very simple and the so-called independent atom model (IAM) used in conventional electron diffraction can be utilized to calculate the DCS. For molecules composed of light atoms, it was shown in Xu *et al* [57] that the DCS of the HATI electrons calculated using IAM is accurate for collision energies around 100 eV. Such electrons can be generated with mid-infrared lasers of wavelength of a few microns.

The use of laser generated HATI electron momentum spectra to probe the interatomic separations of atoms in a molecule is called LIED. In LIED interatomic separations can be extracted in the same manner as in the conventional electron diffraction. Although LIED has been coined much earlier in the era of Ti-Sapphire lasers [58, 59], it was then used at a qualitative level and the method has not been really put to use to extract accurate bond length. With the advent of mid-infrared lasers, LIED experiment was first carried out in 2012 for N_2 and O_2 [60]. Later it was used to extract the bond lengths in C_2H_2 [61] and C_6H_6 [62], with accuracy of the order of 0.05 Å. In the case of hydrocarbon molecules, not only the C–C bond length is accurately retrieved but also the C–H bond length. In the context of the three-step model, the bond length extracted is considered to be the bond length at the time of recollision. In the LIED experiment of Blaga *et al* [60] the O–O distance was found to be about 0.1 Å shorter than the equilibrium distance of neutral oxygen molecule. The result is understood that O–O distance shrinks after one electron is removed. Since it takes about 5 fs for the electron to return to recollide with the O_2^+ ion after ionization, this experiment measures a bond change of 0.1 Å within 5 fs, thus demonstrating for the first time the observation of a dynamic system with sub-angström spatial and few-femtosecond temporal resolutions. Similar method was used to obtain the breaking up of $C_2H_2^+$ molecular ions in the time scale of a few femtoseconds [63].

Looking ahead, the potential of LIED for probing ultrafast dynamics of a molecule still yet to be fully realized. Mid-infrared lasers are readily available already today. Further development in laser technology such as high-repetition rates (hundreds kHz to few MHz) mid-infrared lasers will facilitate the application of LIED for probing femtosecond molecular dynamics, to complement alternative approaches such as ultrafast x-ray diffraction or ultrafast electron diffraction. These latter methods are sensitive to heavy atoms in the molecule. The LIED uses low-energy electrons, thus it is also sensitive to light atoms. It is suitable for probing phenomena such as isomerization, proton transfer and roaming in chemical processes. One can expect that LIED to play an important role as studies of dynamic imaging continue to evolve in the coming years.

4.2. Applications to HHG

HHG is un-disputably the most important topic in strong field rescattering physics. Today, it is the only practical means of generating single attosecond pulses or attosecond pulse trains for applications, covering photons ranging from few tens eVs to sub-keVs. It also offers the possibility of providing tunable table-top coherent light sources over a broad spectral region in small laboratories that are available today only at large-scale national facilities.

According to the QRS theory, HHG also offers the opportunity to extract PRTD over a broadband in a single experiment, to provide information comparable to those

obtained using conventional photoionization experiments. In particular, HHG from partially oriented/aligned molecules can be used to probe molecular frame photoelectron angular distributions that bear the most fundamental properties of molecules. The study of such molecular spectral features using HHG has been generally called HHG spectroscopy.

Experimentally, high-order harmonics observed in the laboratory are generated coherently from all the molecules within the focused laser beam. Under the ideally perfect phase matching condition, the experimental HHG spectra can be used to extract the amplitude and phase of the PRTD of a single molecule. However, it is practically not possible to reach perfect phase matching over a broad spectral region. Still, under low pressure and weak laser intensity condition, the phase and amplitude of the PRTD in the molecular frame have been accurately retrieved from the harmonic spectra of N_2 [64] and a number of other small molecules. Extension of HHG spectroscopy to very high precision or to complex molecules would encounter difficulties. Since QRS is a model based on the single electron picture, or in general, a single-channel, complicated electron correlation among the channels at a fixed nuclear geometry, or coupling between electron and nuclear dynamics, all could render the failure of the simple QRS model. Extension of the QRS model to include these additional couplings is not yet available.

Although straightforward generalization of the QRS concept has been extended to interpreting HHG from complex molecules or to dynamic systems [65], such models often rely on additional approximations that need to be carefully examined. In addition, dynamics such as hole hopping or charge migration have been discussed and 'extracted' in the literature based on modeling, such 'virtual information' are not measurable quantities. A theory of extracting structure information from HHG beyond simple molecular systems will continue to face great challenge due to its complexity.

The strength of the QRS theory for HHG lies in its simplicity where the role of the laser pulse and the target can be separated. As the technology of ultrafast lasers improves, high-order harmonics are being generated with increasing control, including the range of laser wavelength, polarization and phase, as well as optical manipulation. For applications, clearly one would like to increase the harmonics yield, the energy of usable harmonics to water-window region and beyond, or to enhance specific range of harmonics, to replace the need of going to large facilities, or to have such lights available to greater number of users. For such purposes, the enhancement can occur at the single atom level, or at the macroscopic phase matching level. Since phase matching is a very complicated problem that requires extensive simulations based on the solution of Maxwell equations in the macroscopic propagation medium, a fast QRS method of calculating laser-induced dipole is very useful. To increase the output of high harmonics, recent experiments favor high-pressure gas medium and sometimes high laser intensities. Under such generating conditions, the driving laser pulses are drastically modified during the propagation in the gas medium. The QRS theory offers the simplest method to account for the generation of harmonics by a single atom. The other simple model used is the SFA2 theory, but in situations where ionization becomes non-negligible, the simple SFA2 is not adequate as depletion becomes large.

Extensive simulations on HHG generation for optimizing single atom harmonics and for optimizing propagation effect have been carried out by the authors, for example, see [66, 67], and a number of the simulations have been applied to experimental measurements [68, 69]. Still, only a very small number of possibilities have been examined. In particular, very few simulations incorporate manipulation of polarization of individual pulses so far. QRS will continue to play a role in the modeling of the generation of harmonics in the years to come.

4.3. Application to laser pulse characterization

Full characterization of an intense short laser pulse used in a given experiment is a nontrivial matter. Within the focused volume, the electric fields are not determined directly. Assuming that the focused beam is Gaussian in the propagation as well as the transverse direction, one would still need to know the Rayleigh length and the beam radius. For the time profile, FROG or SPIDER can be used to characterize the pulse, but such methods cannot determine the absolute value of the CEP. For a narrow-band transform-limited short pulse, the laser field may be written as

$$E(t) = a(t)\cos(\omega t + \phi), \tag{23}$$

where ω is the angular frequency of the carrier wave, $a(t)$ is the electric field amplitude (the envelope) and ϕ is the CEP. If $a(t)$ is Gaussian, then the absolute value of $a(t)$ can be determined if the power of the laser beam is measured. Using conventional optical methods, however, the CEP cannot be determined.

Following the QRS model, the wave packet $W(p_r)$ can be extracted if the DCS for the atomic target is known, for example, for rare gas atoms. The $W(p_r)$ clearly will depend on ϕ, and the asymmetry of electron emission along the 'left' and 'right' sides of the polarization axis clearly will depend on ϕ. In principle, one can retrieve the CEP from the asymmetry of the HATI spectra. However, in real experiments, the pulse duration is not known precisely either, nor is the laser intensity. Thus even if the laser intensity is uniform in space, as described by equation (23), for example, the intensity, pulse duration and CEP have to be retrieved at the same time. When the CEP of the laser is not stabilized, the left/right electron spectra along the polarization axis can be collected and analyzed shot by shot. By analyzing the so-called asymmetry ellipse [70] of the wave packet $W(p_r)$ on the two sides, the CEP of each single shot can be determined, see Chen *et al* [71]. In recent years, CEP stabilized short pulses are commercially available but the actual CEP is still not known. In this case a different method of retrieving the CEP, laser peak intensity, and pulse duration has been proposed recently [72]. The iterative retrieval method relies on generating a large number of HATI spectra to identify which best

fits the experimental data. Thus a fast method of calculating HATI spectra like QRS is essential.

Asymmetric left/right angular distributions of HATI electrons can also be expected from a two-color laser pulse. The relative phase between the two colors can also be determined using the same idea, see for example, Ray *et al* [73]. In the future, the QRS can also be used to extract pulses that are not linearly polarized since the QRS has been shown to apply to any other polarizations, see section 3.6.

To generate single attosecond pulses or to enhance high-harmonic yields, synthesized waves as short as one femtosecond duration are obtained by combining multiple short pulses [74]. They can also be obtained by supercontinuum generated in a hollow fiber, or by multiple plates in the air. Such broadband IR or mid-IR pulses may be characterized also using the QRS theory. Alternative methods would be to use the analog of attosecond streaking like PROBP, which is similar to FROG-CRAB but without the limitation of the FROG-CRAB, see Zhao *et al* [75]. This topic has not been widely explored yet.

4.4. Application to NSDI

NSDI involves at least two free electrons at the end of the process. In the context of the QRS model, the $W(p_r)$ is obtained from a one-electron process so it can be obtained from the HATI spectra. On the other hand, electron impact ionization, e-$2e$, is a two-electron process. Within the QRS model, for each returning electron with kinetic energy $E_r = p_r^2/2$, the e-$2e$ impact ionization cross section can be calculated using the time-independent scattering theory. Depending on whether the measurement is total NSDI or the correlated electron momentum spectra, suitable $W(p_r)$-weighted integration over the energy of the returning electron has to be carried out. In addition, since NSDI is highly nonlinear, meaning that it changes rapidly with laser intensity, volume integration over the focused beam should be carried out if the theory is to compare with experiments.

In NSDI, two electrons ejection can also occur through electron impact excitation followed by ionization from the excited states by the laser. Thus electron impact excitation cross sections are also needed. The latter can also be calculated accurately using electron impact excitation codes. For the subsequent ionization of the excited electron, one can use tunnel ionization model or over-the-barrier-ionization model [76].

So far, most of the NSDI experiments are simulated with the classical theory. The QRS theory has been applied in a few cases but with electron impact excitation and e-$2e$ ionization cross sections obtained from simple models. More recently, such cross sections for helium target have been calculated using the state-of-the-art R-matrix code, thus NSDI involving helium target has been revisited using the QRS theory. For instance, the intensity dependence of the ratio of double to single ionization in the NSDI region using 780 nm laser has been carried out using the QRS theory [77]. The agreement with experiment has been found to be very good.

In NSDI calculation, a large amount of electron-impact excitation and electron-impact ionization cross sections are needed. To perform QRS-type calculation, additional assumption on the core electrons has to be considered. For example, the suppression of the ionization threshold of the second electron by the laser has to be account for, see [78]. The prototype of such calculations can be found in [77].

5. Summary and conclusions

Nearly twenty-five years ago, the recollision model began to form the basic foundation for understanding many important and pioneering experiments in strong field physics. In its first fifteen years, the model was used mostly for 'interpreting' the observed results. The initial recollision model did not offer a recipe for calculating electron dynamics that is consistent with the quantum theory. Since recollision happens in the presence of the laser field, precisely how to describe electron–ion recollision was left answered. The development of the QRS theory around 2007–2009 has changed that significantly. Within the QRS model, it has clearly established that electron–ion recollision happens under the field-free condition. With the QRS, the recollision model is not only simple to understand, but also rather simple to calculate with high precision.

In the last eight or so years we have witnessed extensive applications of the QRS model. Still, the model is not complete as complexity and degrees of freedom in the system grows. For example, it is still largely unclear how to properly incorporate electron-nuclear coupling within the QRS scheme [79]. Today, QRS remains to be the only widely applicable simple model for making quantitative predictions on recollision phenomena. The only other alternatives are mostly based on brute-force numerical solution of the TDSE in one way or another.

Acknowledgments

This work was supported by the Chemical Sciences, Geosciences and Biosciences Division, Office of Basic Energy Sciences, Office of Science, US Department of Energy under Grant No. DE-FG02-86ER13491. CJ was supported by Fundamental Research Funds for the Central Universities of China under Grant NO. 30916011207, and by National Natural Science Foundation of China under Grant No. 11774175. The authors also wish to acknowledge contributions from Xiao-Min Tong, Zengxiu Zhao, Toru Morishita, Zhangjin Chen and Junliang Xu who all have helped the development of the QRS theory reported here in the years back.

ORCID iDs

C D Lin https://orcid.org/0000-0003-4847-8938
Anh-Thu Le https://orcid.org/0000-0003-3577-4180
Hui Wei https://orcid.org/0000-0001-7199-4434

References

[1] Chen Z, Le A-T, Morishita T and Lin C D 2009 *Phys. Rev.* A **79** 033409
[2] Le A-T, Lucchese R R, Tonzani S, Morishita T and Lin C D 2009 *Phys. Rev.* A **80** 013401
[3] Kuchiev M Y 1987 *JETP Lett.* **45** 404
[4] Krause J L, Schafer K J and Kulander K C 1992 *Phys. Rev. Lett.* **68** 3535
[5] Corkum P B 1993 *Phys. Rev. Lett.* **71** 1994
[6] Lewenstein M, Balcou P, Ivanov M Y, L'Huillier A and Corkum P B 1994 *Phys. Rev.* A **49** 2117
[7] Keldysh L 1965 *JETP Sov. Phys.* **20** 1307
[8] Faisal F H M 1973 *J. Phys. B: At. Mol. Phys.* **6** L89
[9] Reiss H R 1980 *Phys. Rev.* A **22** 1786
[10] Muth-Böhm J, Becker A and Faisal F H M 2000 *Phys. Rev. Lett.* **85** 2280
[11] Ammosov M, Delone N and Krainov V 1986 *JETP Sov. Phys.* **64** 1191
[12] Tong X M, Zhao Z X and Lin C D 2002 *Phys. Rev.* A **66** 033402
[13] Alnaser A S, Voss S, Tong X M, Maharjan C M, Ranitovic P, Ulrich B, Osipov T, Shan B, Chang Z and Cocke C L 2004 *Phys. Rev. Lett.* **93** 113003
[14] Zhou X X, Tong X M, Zhao Z X and Lin C D 2005 *Phys. Rev.* A **71** 061801
[15] Zhou X, Tong X M, Zhao Z X and Lin C D 2005 *Phys. Rev.* A **72** 033412
[16] Itatani J, Levesque J, Zeidler D, Niikura H, Pepin H, Kieffer J C, Corkum P B and Villeneuve D M 2004 *Nature* **432** 867
[17] Kanai T, Minemoto S and Sakai H 2005 *Nature* **435** 470
[18] Le A-T, Tong X-M and Lin C D 2006 *Phys. Rev.* **73** 041402
[19] Paul P M, Toma E S, Breger P, Mullot G, Augé F, Balcou P, Muller H G and Agostini P 2001 *Science* **292** 1689
[20] Hentschel M, Kienberger R, Spielmann C, Reider G A, Milosevic N, Brabec T, Corkum P, Heinzmann U, Drescher M and Krausz F 2001 *Nature* **414** 509
[21] Yang B, Schafer K J, Walker B, Kulander K C, Agostini P and DiMauro L F 1993 *Phys. Rev. Lett.* **71** 3770
[22] Spanner M, Smirnova O, Corkum P B and Ivanov M Y 2004 *J. Phys. B: At. Mol. Opt. Phys.* **37** L243
[23] Le V-H, Le A-T, Xie R-H and Lin C D 2007 *Phys. Rev.* A **76** 013414
[24] Morishita T, Chen Z, Watanabe S and Lin C D 2007 *Phys. Rev.* A **75** 023407
[25] Chen Z, Morishita T, Le A-T, Wickenhauser M, Tong X M and Lin C D 2006 *Phys. Rev.* **74** 053405
[26] Chen Z, Morishita T, Le A-T and Lin C D 2007 *Phys. Rev.* **76** 043402
[27] Morishita T, Le A-T, Chen Z and Lin C D 2008 *Phys. Rev. Lett.* **100** 013903
[28] Perelomov A M, Popov V S and Terent'ev M V 1966 *Sov. Phys.—JETP* **23** 924
[29] Le A-T, Morishita T and Lin C D 2008 *Phys. Rev.* **78** 023814
[30] Trallero-Herrero C, Jin C, Schmidt B E, Shiner A D, Kieffer J-C, Corkum P B, Villeneuve D M, Lin C D, Legare F and Le A-T 2012 *J. Phys. B: At. Mol. Opt. Phys.* **45** 011001
[31] Cerkic A, Hasovic E, Milosevic D B and Becker W 2009 *Phys. Rev.* A **79** 033413
[32] Frolov M V, Manakov N L and Starace A F 2009a *Phys. Rev.* A **79** 033406
[33] Frolov M V, Manakov N L, Sarantseva T S, Emelin M Y, Ryabikin M Y and Starace A F 2009 *Phys. Rev. Lett* **102** 243901
[34] Tolstikhin O I, Morishita T and Watanabe S 2010 *Phys. Rev.* A **81** 033415
[35] Zhou X, Chen Z, Morishita T, Le A-T and Lin C D 2008 *Phys. Rev.* **77** 053410
[36] Morishita T and Tolstikhin O I 2017 *Phys. Rev.* A **96** 053416
[37] Le A-T, Wei H, Jin C and Lin C D 2016 *J. Phys. B: At. Mol. Opt. Phys.* **49** 053001
[38] Frolov M V, Manakov N L, Sarantseva T S and Starace A F 2012 *Phys. Rev.* A **86** 063406
[39] Frolov M V *et al* 2016 *Phys. Rev.* A **93** 031403
[40] Sarantseva T S, Frolov M V, Manakov N L, Ivanov M Y and Starace A F 2013 *J. Phys. B: At. Mol. Opt. Phys.* **46** 231001
[41] Fleischer A, Kfir O, Diskin T, Sidorenko P and Cohen O 2014 *Nat. Photon.* **8** 543
[42] Kfir O *et al* 2014 *Nat. Photon.* **9** 99
[43] Fan T *et al* 2015 *Proc. Natl Acad. Sci. USA* **112** 45
[44] Mancuso C A *et al* 2015 *Phys. Rev.* A **91** 031402
[45] Mancuso C A *et al* 2016 *Phys. Rev.* A **93** 053406
[46] Baykusheva D, Ahsan M S, Lin N and Wörner H J 2016 *Phys. Rev. Lett.* **116** 123001
[47] Medišauskas L, Wragg J, van der Hart H and Ivanov M Y 2015 *Phys. Rev. Lett.* **115** 153001
[48] Milošević D B 2015 *Phys. Rev.* A **92** 043827
[49] Hoang V-H, Le V-H, Lin C D and Le A-T private communication
[50] Hoang V-H, Le V-H, Lin C D and Le A-T 2017 *Phys. Rev.* A **95** 031402
[51] Lin C D, Le A-T, Jin C and Wei H 2018 *Attosecond and Strong Field Physics* (Cambridge: Cambridge University Press) in press
[52] Okunishi M, Lucchese R, Morishita T and Ueda K 2014 *J. Electron Spectrosc. Relat. Phenom.* **195** 313
[53] Tate J, Auguste T, Muller H G, Salières P, Agostini P and DiMauro L F 2007 *Phys. Rev. Lett.* **98** 013901
[54] Schiessl K, Ishikawa K L, Persson E and Burgdörfer J 2007 *Phys. Rev. Lett.* **99** 253903
[55] Frolov M V, Manakov N L and Starace A F 2008 *Phys. Rev. Lett.* **100** 173001
[56] Le A-T, Wei H, Jin C, Tuoc V N, Morishita T and Lin C D 2014 *Phys. Rev. Lett.* **113** 033001
[57] Xu J, Chen Z, Le A-T and Lin C D 2010 *Phys. Rev.* A **82** 033403
[58] Zuo T, Bandrauk A and Corkum P 1996 *Chem. Phys. Lett.* **259** 313
[59] Meckel M *et al* 2008 *Science* **320** 1478
[60] Blaga C I, Xu J, DiChiara A D, Sistrunk E, Zhang K, Agostini P, Miller T A, DiMauro L F and Lin C D 2012 *Nature* **483** 194
[61] Pullen M, Wolter B, Le A-T, Matthias Baudisch A M H, Senftleben A, Schröter C D, Ullrich J, Moshammer R, Lin C D and Biegert J 2015 *Nat. Commun.* **6** 7262
[62] Ito Y, Wang C, Le A-T, Okunishi M, Ding D, Lin C D and Ueda K 2016 *Struct. Dyn.* **3** 034303
[63] Wolter B *et al* 2016 *Science* **354** 308
[64] Ren X, Makhija V, Le A-T, Troß J, Mondal S, Jin C, Kumarappan V and Trallero-Herrero C 2013 *Phys. Rev.* A **88** 043421
[65] Kraus P M *et al* 2015 *Science* **350** 790
[66] Jin C, Wang G, Wei H, Le A-T and Lin C D 2014 *Nat. Commun.* **5** 4003
[67] Jin C, Wang G, Le A-T and Lin C D 2014 *Sci. Rep.* 7067
[68] Jin C and Lin C D 2016 *Phys. Rev.* A **94** 043804
[69] Sun H-W, Huang P-C, Tzeng Y-H, Huang J-T, Lin C D, Jin C and Chen M-C 2017 *Optica* **4** 976
[70] Wittmann T, Horvath B, Helml W, Schätzel M G, Gu X, Cavalieri A L, Paulus G G and Kienberger R 2009 *Nat. Phys.* **5** 357
[71] Chen Z, Wittmann T, Horvath B and Lin C D 2009 *Phys. Rev.* A **80** 061402
[72] Zhou Z, Wang X, Chen Z and Lin C D 2017 *Phys. Rev.* A **95** 063411

[73] Ray D, Chen Z, De S, Cao W, Litvinyuk I V, Le A T, Lin C D, Kling M F and Cocke C L 2011 *Phys. Rev.* A **83** 013410
[74] Wirth A *et al* 2011 *Science* **334** 195
[75] Zhao X, Wei H, Wu Y and Lin C D 2017 *Phys. Rev.* A **95** 043407
[76] Tong X M and Lin C D 2005 *J. Phys. B: At. Mol. Opt. Phys.* **38** 2593
[77] Chen Z *et al* 2015 *Phys. Rev.* A **92** 063427
[78] van der Hart H W and Burnett K 2000 *Phys. Rev.* A **62** 013407
[79] Le A-T, Morishita T, Lucchese R R and Lin C D 2012 *Phys. Rev. Lett.* **109** 203004